The current issue and full text archive of this journal is available at
www.emeraldinsight.com/0961-5539.htm

Numerical simulation of three-dimensional interfacial flows

E. Jahanbakhsh, R. Panahi and M.S. Seif
Marine Laboratory, Department of Mechanical Engineering, Sharif University of Technology, Tehran, Iran

Abstract

Purpose – This study aims to present compatible computational fluid dynamics procedure for calculation of incompressible three-dimensional time-dependent flow with complicated free surface deformation. A computer software is developed and validated using a variety of academic test cases.

Design/methodology/approach – Two fluids are modeled as a single continuum with a fluid property jump at the interface by solving a scalar transport equation for volume fraction. In conjunction, the conservation equations for mass and momentum are solved using fractional step method. Here, a finite volume discretisation and colocated arrangement are used.

Findings – The developed code results in accurate simulation of interfacial flows, e.g. Rayleigh-Taylor instability, sloshing and dambreaking problems. All results are in good concordance with experimental data especially when there are two phases with high density ratio.

Research limitations/implications – Turbulence, which has great importance in a wide variety of real world phenomena, is not considered in the present formulation and left for future researches.

Originality/value – Here, an integrated numerical simulation for transient interfacial flows is presented. In this way, the pressure integral term in Navier-Stokes equation is discretised based on a newly developed interpolation which results in non-oscillative velocity field especially in free surface.

Keywords Flow measurement, Numerical control, Density measurement, Simulation

Paper type Research paper

1. Introduction

Interfacial flows play a very important role in many physical processes in a variety of domains. While nowadays the single-phase flow simulation tools are widely used both for engineering and research purposes, the simulation of two-phase flow is still considerably a complex problem. However, the continuous growth of computer power strongly helps researchers to apply different formulations and to develop the CFD codes capable of predicting such complex flows. This case is always divided into two main subproblems:

- Navier-Stokes and continuity equations or velocity and pressure distribution; and
- free surface modeling.

Methods for solving the Navier-Stokes and continuity equations are typically categorized as:

- pressure-corrector schemes; and
- projection or fractional step schemes.

In pressure corrector methods like SIMPLE (Patankar and Spalding, 1972) and PISO (Issa, 1986; Versteeg and Malalasekera, 1995), a pressure correction equation is solved

International Journal of Numerical Methods for Heat & Fluid Flow
Vol. 17 No. 4, 2007
pp. 384-404
© Emerald Group Publishing Limited
0961-5539
DOI 10.1108/09615530710739167

for several times in each time step to reach a divergence free velocity field. In contrast with such iterative methods, in fractional step schemes a pressure or pseudo-pressure Poisson equation is solved once in each time step to enforce continuity. Therefore, using such schemes is preferable, especially in unsteady problems (Ferziger and Peric, 2002).

Fractional step methods which have been used widely over past two decades, pioneered by Chorin (1968, 1969) based on Hodge decomposition. In the 1980s, several second-order projection methods are proposed by Goda (1979), Kim and Moin (1985), Van Kan (1986) and Bell *et al.* (1991). Accuracy of such methods were discussed by Brown *et al.* (2001), resulted in introducing a modified scheme based on Bell *et al.* (1991). This method has second-order time accuracy for both pressure and velocity.

On the other hand, the existing approaches for handling fluids interface (Muzaferija and Peric, 1998) are:

- interface tracking or surface methods; and
- interface capturing or volume methods.

Interface tracking methods are characterized by an explicit representation of the interface. In other words, the computational grid is moved and updated in each time step to have no flow across it while satisfying force equilibrium on fluid at interface which are kinematic and dynamic conditions, respectively (Ferziger and Peric, 2002). The common drawback of this category is the inability to handle complicated deformations, e.g. overturning waves. This problem leads to interface capturing methods where the interface is captured as a part of the physical domain. One of the most interesting approaches in volume methods is to solve an additional convection equation. This results in volume fraction which implies the availability of two phases in each control volume (CV) for whole domain. In discretisation of such a transport equation one encounters to face values which must be estimated using an appropriate interpolation scheme. This interpolation must ensure both boundedness and availability criteria (Ubbink, 1997) to have physical volume fraction values. It means that, the value of a flow property in the absence of source or sink cannot be higher or lower than prescribed on the boundaries of a cell. In addition, the amount of flow convected over a face during a time step should be less than or equal to the amount available in doner cell. Simple interpolations have some problem with transitional area between two phases while introducing numerical diffusion (Leonard, 1991) or disobeying the local boundedness (Leonard, 1979). There are some composite schemes which are switching between their options according to the received signals about the current, to have physical distribution of fluids in whole domain (Ubbink and Issa, 1999; Dendy *et al.*, 2002). Compressive interface capturing scheme for arbitrary meshes (CICSAM) (Ubbink and Issa, 1999) is a promising method which appropriately retains the transitional region between two phases while successfully establishes all criteria – especially mass conservation which is the common drawback of volume methods – in comparison to other composite interpolations (Panahi *et al.*, 2005).

The objective of this study is simulation of the three-dimensional interfacial flow with complex deformation of free surface. This subject is recently developed by many researchers especially based on interface capturing methods (Scardovelli and Zaleski, 1999; Jahanbakhsh *et al.*, 2005) and used to simulate breaking waves (Chen and Kharif, 1999; Biausser *et al.*, 2004), green water (Fekken *et al.*, 1999; Huijsmans and Van Grosen, 2004), sloshing (Loots *et al.*, 2004) and wave-structure interaction (Yang *et al.*, 2005).

In this study, a finite volume solver is developed based on using CICSAM interpolation for volume fraction transport equation and fractional step method for velocity and pressure coupling. Complexity of flow and high density ratio of two phases lead to appropriate discretisations treated innovatively in this paper especially for pressure term.

Finally, computer software is developed based on the mentioned algorithm and verified using Raleigh-Taylor instability, sloshing in a rectangular tank and dam breaking problem with and without obstacle.

2. Numerical method

2.1 Governing equations

There is an approach in simulation of two-phase flow where different fluids are modeled as a single fluid obeying the same set of governing equations, with the different local identified volume fraction values α. Incompressible Navier-Stokes and continuity equations are well-known and given by the equations:

$$\frac{\partial u_i}{\partial t} + u_j \frac{\partial u_i}{\partial x_j} = -\frac{1}{\rho}\frac{\partial P}{\partial x_i} + \nu \frac{\partial^2 u_i}{\partial x_j \partial x_j} + g_i \tag{1}$$

$$\frac{\partial u_i}{\partial x_i} = 0 \tag{2}$$

where u_i is the velocity, P is the pressure, and ν is the kinematic viscosity.

Local density ρ and viscosity ν of the single fluid are defined as:

$$\begin{aligned} \rho_{\text{cell}} &= \alpha\rho_1 + (1-\alpha)\rho_2 \\ \nu_{\text{cell}} &= \alpha\nu_1 + (1-\alpha)\nu_2 \end{aligned} \tag{3}$$

Subscripts 1 and 2 indicate two fluids (e.g. water and air), where α (volume fraction) is the percentage of fluid 1 (e.g. water) available in cell and defined as follow:

$$\alpha = \begin{cases} 1 & \text{for cells inside fluid 1} \\ 0 & \text{for cells inside fluid 2} \\ 0 < \alpha_0 < 1 & \text{for transitional area} \end{cases} \tag{4}$$

Reformulating the continuity equation (2) and using the definition of the single fluid density, results in extracting a scalar transport equation for volume fraction α (Spalding, 1974):

$$\frac{\partial \alpha}{\partial t} + \vec{\nabla}(\alpha \vec{u}) = 0 \tag{5}$$

2.2 Discretisation

Discretisation of the governing equations is considered by integration of the momentum equation over a control volume it becomes as below:

$$\frac{\mathrm{d}}{\mathrm{d}t}\int_V \vec{u}\,\mathrm{d}V + \int_A \vec{u}(\vec{u}\vec{n})\,\mathrm{d}A = \int_A \nu\vec{\nabla}\vec{u}\vec{n}\,\mathrm{d}A - \frac{1}{\rho}\int_A P\vec{n}\,\mathrm{d}A + \int_V \vec{g}\mathrm{d}V \tag{6}$$

where $\vec{u}$ is the velocity vector, ν is the cell volume and A is the area around it.

The diffusion term (the first term in r.h.s. of equation (6)) is discretised using the over-relaxed interpolation for velocity component u_i (Jasak, 1996):

$$\int_A \nu\vec{\nabla}u_i\vec{n}\,\mathrm{d}A = \sum_{f=1}^{n} \nu_f\vec{A}_f(\vec{\nabla}u_i)_f \tag{7}$$

where $\vec{A}_f$ is the CV face area vector.

Discretisation of the convection term (the second term in l.h.s. of equation (6)) needs to the fluid velocity component on CV face $u_{i\text{-}f}$ as shown in equation (8):

$$\int_A u_i(\vec{u}\vec{n})\mathrm{d}A = \sum_{f=1}^{n} u_{i-f}F_f \tag{8}$$

where $F_f = \vec{A}_f\vec{U}_f$ is the volumetric flux. The fluid velocity on CV face $\vec{U}_f$ must be calculated separately in the colocated arrangement to avoid checkerboard pressure and will be discussed later in the solution algorithm. Here, u_{i-f} is approximated using gamma interpolation scheme (Jasak, 1996) based on normalized variable diagram (NVD) (Leonard, 1991) concept:

$$u_{i-f} = \begin{cases} u_{i-D} & \text{for } \tilde{u}_{i-D} \le 0 \text{ or } \tilde{u}_{i-D} \ge 1 \\ \dfrac{1}{2}(u_{i-D} + u_{i-A}) & \text{for } k \le \tilde{u}_{i-D} < 1 \\ \left(1 - \dfrac{\tilde{u}_{i-D}}{2k}\right)u_D + \frac{\tilde{u}_{i-D}}{2k}u_{i-A} & \text{for } 0 \le \tilde{u}_{i-D} < k \end{cases} \tag{9}$$

Subscripts D and A stand for doner and acceptor cells determined for each CV's face according to the direction of flow as shown in Figure 1. In addition, $\tilde{\phi}_D$and $\tilde{\phi}_f$ are defined based on NVD as equations (10) and (11):

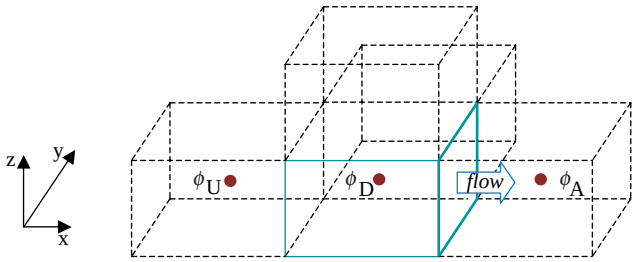

Figure 1.
Flow direction (arrow) determines doner, acceptor and upwind cells for each CV's face

$$\tilde{\phi}_D = \frac{\phi_D - \phi_U}{\phi_A - \phi_U} \tag{10}$$

$$\tilde{\phi}_f = \frac{\phi_f - \phi_U}{\phi_A - \phi_U} \tag{11}$$

It must be mentioned that the Crank-Nicholson scheme is used for time discretisation of diffusion and convection terms in momentum equation (6).

The pressure term (second term in r.h.s. of equation (6)) is discretised as equation (12):

$$\int_A P\vec{n}\,\mathrm{d}A = \sum_{f=1}^{n} P_f \vec{A}_f \tag{12}$$

Using the common linear interpolations (LI) for calculation of face pressure P_f, results in severe oscillations in velocity field. This is of great importance, especially when there are two fluids with high density ratio, e.g. water and air. Here a piecewise linear interpolation (PLI) shown in Figure 2 is introduced and used for P_f estimation. It is based on a constraint for lines L_{Af} and L_{Bf} which connect pressure values at CVs' center P_A and P_B to P_f as equation (13):

$$\frac{\text{Slope of } L_{Af}}{\text{Slope of } L_{Bf}} = \frac{\rho_A}{\rho_B} \tag{13}$$

where ρ_A and ρ_B are the densities of CVs A and B, respectively.

Therefore, P_f can be estimated by using the pressure value at CVs' center P_A and P_B as well as equation (14):

$$P_f = P_A\kappa + P_B(1 - \kappa) \tag{14}$$

κ is the weighting factor and can be calculated as equation (15):

$$\kappa = \frac{\rho_B \delta_B}{\rho_A \delta_A + \rho_B \delta_B} \tag{15}$$

where δ_A and δ_B are distance from face center f to CVs' center A and B, respectively (Figure 2).

In order to show the effect of such an interpolation, the hydrostatic pressure distribution along the near free surface cells (Figure 3(a)) is plotted in Figure 3(b). In Figure 3(a) points and solid lines stand for CV's centers and faces, respectively.

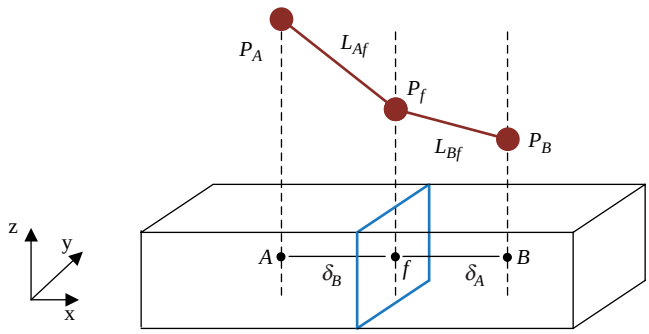

Figure 2.
PLI for CV's face pressure calculation

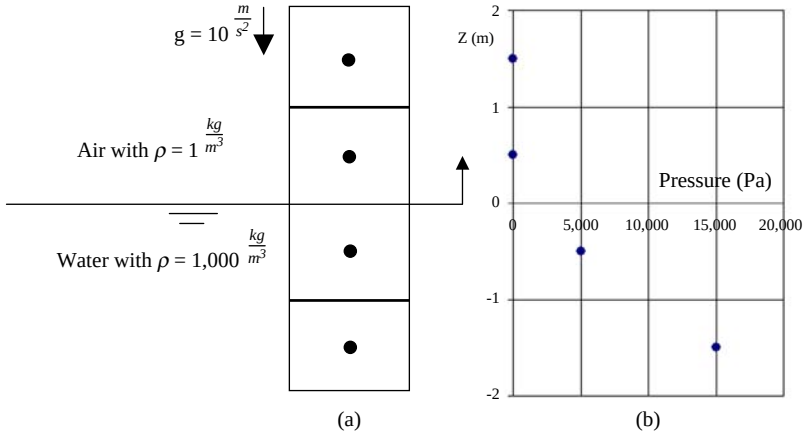

Figure 3.
Hydrostatic pressure distribution at near free surface CVs' centers

Figure 4 shows the pressure distribution at CVs' faces calculated by using LI and PLI. It is obvious from Figure 4 that using LI results in non-physical pressure at CV's face, but PLI calculates the CV's face pressure exactly which is zero for the face at $x = 0$ m. This difference effects on pressure integral of each CV consequently, as shown in Figure 5. Although it seems that such a difference by using LI in comparison to PLI can be neglected, dividing of pressure integral term by CV's density (equation (6)) exaggerates this error, especially in the case of large density ratio of two phases and for the CV next to the free surface in the light fluid (here at $Z = 0.5$ m). Therefore, using PLI restrains severe oscillations of the velocity field by better estimation of P_f.

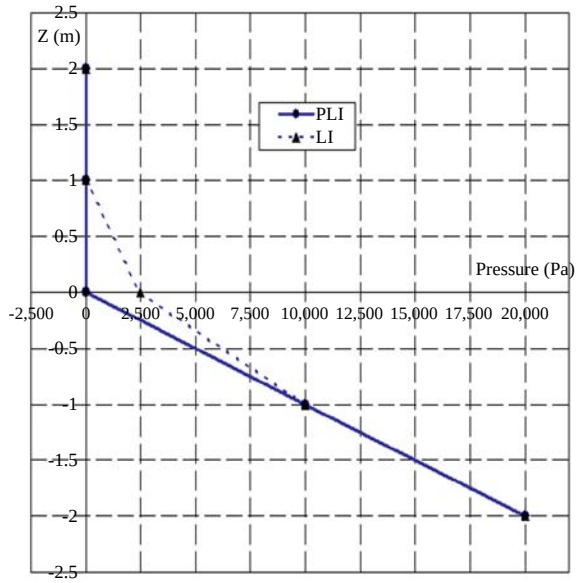

Figure 4.
Pressure at CVs' centers and faces

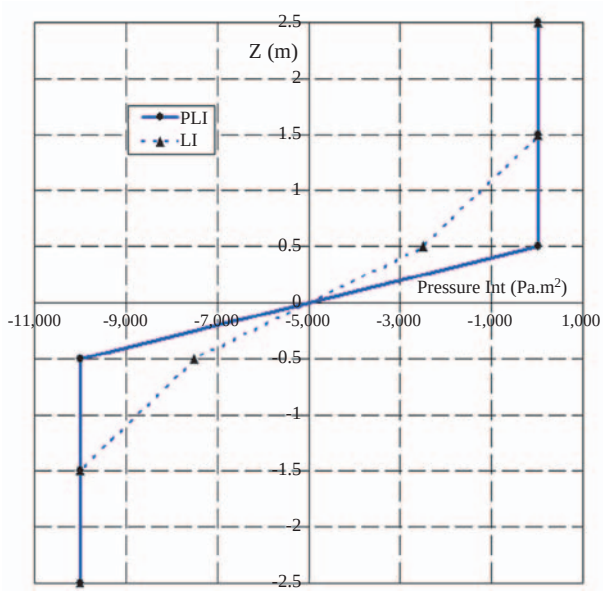

Figure 5.
Pressure integral

Finite volume discretisation of volume fraction transport equation (5) is based on the integration over CV and time step:

$$\int_t^{t+\delta t}\left(\int_V \frac{\partial \alpha}{\partial t}\mathrm{d}v\right)\mathrm{d}t + \int_t^{t+\delta t}\left(\int_V \vec{\nabla}(\alpha\vec{u})\mathrm{d}V\right)\mathrm{d}t = 0 \tag{16}$$

The first term in equation (16) is a common integral form and applying the Gauss theorem on the second term results in:

$$\left(\alpha_P^{t+\delta t} - \alpha_P^t\right)\frac{V}{\delta t} + \frac{1}{2}\left(\sum_{f=1}^{n}\alpha_f^{t+\delta t}F_f^{t+\delta t} + \sum_{f=1}^{n}\alpha_f^t F_f^t\right) = 0 \tag{17}$$

The time integral of the second term is discretised using Crank-Nicholson scheme. Assuming a linear and small variation of F_f in small time step, results in using the most recent value of it. Taking this into account, and rearranging of equation (17) yield to:

$$\alpha_P^{t+\delta t}\frac{V}{\delta t} + \sum_{f=1}^{n}\frac{1}{2}\alpha_f^{t+\delta t}F_f = S_{\alpha_P} \tag{18}$$

where the source term is:

$$S_{\alpha_P} = \alpha_P^t\frac{V}{\delta t} - \sum_{f=1}^{n}\frac{1}{2}\alpha_f^t F_f \tag{19}$$

One can see the face values α_f which must be approximated using an interpolation. As aforementioned, simple interpolations leads to non-physical or too diffusive volume fraction values. This leads to use a high order composite one. Most of composite methods, typically switch between two high and low order interpolations

to use their advantages. Here, the main distinctions are how and when they switch between these schemes according to flow information.

CICSAM uses convection boundedness criteria (CBC) (Gaskell and Lau, 1988) and ULTIMATE-QUICKEST (UQ) (Leonard, 1991) by introducing a weighting factor γ_f (equation (20)) which takes into account the slope of the free surface relative to the direction of motion. CBC is the most compressive scheme that stipulates robust local bounds on $\tilde{\alpha}_f$ nevertheless does not actually preserve the shape of interface. Here UQ uses for its ability to better preserving of interface shape. Based on NVD, normal face value is obtained as follows:

$$\tilde{\alpha}_f = \gamma_f \tilde{\alpha}_{f_{\mathrm{CBC}}} + (1 - \gamma_f)\tilde{\alpha}_{f_{\mathrm{UQ}}} \tag{20}$$

Using the definition of equation (11) in equation (20), results in estimation of α_f, shown in equation (18). This value contains all the information regarding to the fluid distribution in the doner, acceptor and upwind cells as well as the interface orientation relative to flow direction. To avoid non-physical α in highly skewed meshes, a correction step is added to volume fraction calculation procedure and used in the developed software which can be found in Ubbink and Issa (1999) by details.

2.3 Solution algorithm

Solving the volume fraction transport equations (18) and (19), results in calculation of an effective fluid properties using equation (3). Here, this single fluid is used in coupling of velocity and pressure fields by fractional step method of Brown *et al.* (2001), which is a modified scheme based on Bell *et al.* (1991). The first step is solving the momentum equation for the intermediate velocity u_i^* with the lagged pressure gradient where physical velocity component u_i^n is known from the previous time step:

$$\frac{u_i^* - u_i^n}{\Delta t} = \frac{1}{2}\left[H(u_i)^* + H(u_i)^n\right] - \frac{1}{\rho}G_i(P^{n-1/2}) + K_i \tag{21}$$

where:

$$H(u) = \int_A \nu\vec{\nabla}u_i\vec{n}\,\mathrm{d}A - \int_A u_i(\vec{u}\vec{n})\,\mathrm{d}A \tag{22}$$

$$G_i(P) = \int_A Pn_i\,\mathrm{d}A \tag{23}$$

$$\mathrm{K}_i = \int_V g_i\,\mathrm{d}V \tag{24}$$

Here, $u^*|_{\mathrm{Boundary}} = u^{n+1}|_{\mathrm{Boundary}}$ boundary condition is used for equation (21) which keeps the second order time accuracy for u_i^* (Brown *et al.*, 2001).

The next step is solving a Poisson equation for pressure like variable ϕ with zero gradient boundary condition:

$$\oint_A \frac{1}{\rho}\frac{\partial \phi^{n+1}}{\partial n}\mathrm{d}A = \frac{1}{\Delta t}\oint_A u_i^* \mathrm{d}A \tag{25}$$

Especial care must be taken in calculation of the r.h.s. integral of equation (25) for boundary CVs (Kim and Choi, 2000). In other words, the physical face velocity $\vec{U}_f^n$ calculated in the previous time step must be used on the boundary rather than the intermediate one:

$$\frac{1}{\Delta t}\oint_A u_i^* \mathrm{d}A = \sum_{f \notin \text{Boundary}} \vec{U}_f^* \vec{A}_f + \sum_{f \in \text{Boundary}} \vec{U}_f^n \vec{A}_f x \tag{26}$$

where the intermediate face velocity $\vec{U}_f^*$ is calculated by the linear interpolation of cell center intermediate one.

By using the gradient of ϕ, the physical velocity component is calculated as equation (27):

$$u_i^{n+1} = u_i^* + \frac{\Delta t}{\rho} G(\phi^{n+1}) \tag{27}$$

Decoupling of velocity and pressure fields is the common problem in colocated arrangement which is used in current study. This leads to the especial treatment of face velocities as well as momentum interpolation scheme (Zang *et al.*, 1994; Kim and Choi, 2000). Here, equation (28) is used to overcome this problem:

$$U_f^{n+1} = U_f^* + \frac{\Delta t}{\rho}\frac{\partial \phi^{n+1}}{\partial n} \tag{28}$$

Finally, the pressure is updated as below:

$$P^{n+1/2} = P^{n-1/2} + \phi^{n+1} - \frac{\nu \Delta t}{2}\nabla^2 \phi^{n+1} \tag{29}$$

The last term in equation (29), guarantees the second order time accuracy of pressure in contrast with Bell *et al.* (1991).

3. Test cases and numerical results

In order to assess the feasibility, computer software is written according to above mentioned procedure. This is summarized in some conclusion about the accuracy, efficiency and robustness of such an algorithm.

3.1 The two-dimensional Rayleigh-Taylor problem

When a horizontal layer of heavy fluid overlies a layer of light fluid in the presence of vertical gravitational field, the interface between the two fluids is unstable. In this case, any perturbation grows with time. This phenomenon is known as the Rayleigh-Taylor problem and related computations have been performed by Puckett *et al.* (1997), Kelecy and Pletcher (1997) and later by Popinet and Zaleski (1999).

3.1.1 Rayleigh-Taylor problem with interface perturbation. Here, the interface between two phases is perturbed according to Figure 6. A rectangular domain of 1 m wide, 4 m high, surrounded with wall is discretised using 64 × 256 cells.

The numerical results have been compared to other one obtained by Popinet and Zaleski (1999) in Figure 7 which shows a good concordance.

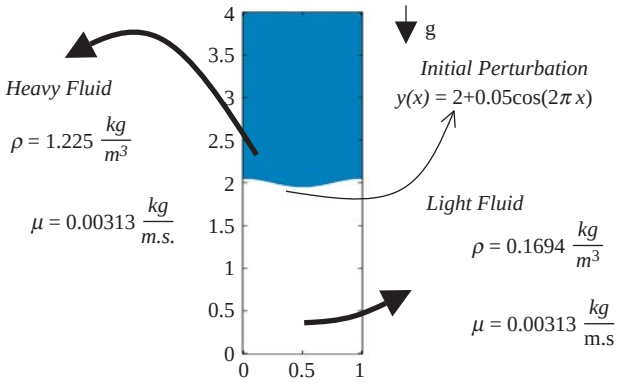

Figure 6.
Illustration of Rayleigh-Taylor problem with interface perturbation

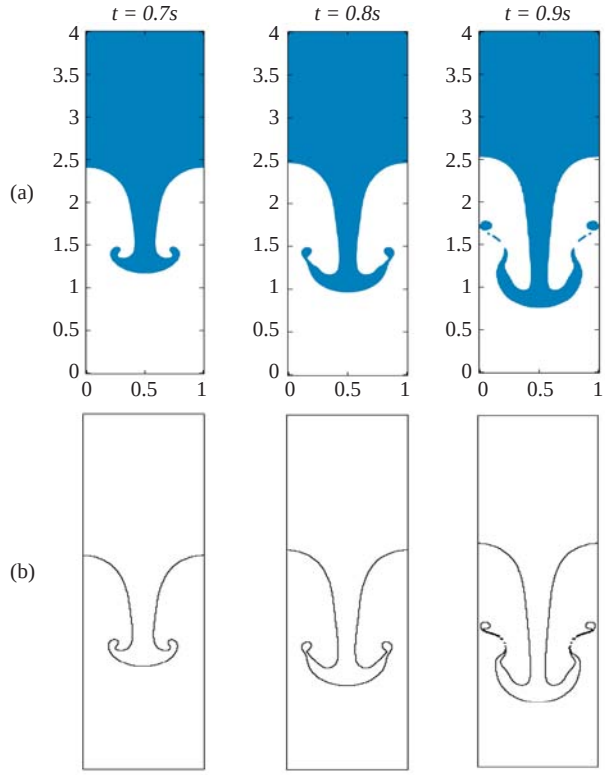

Figure 7.
Rayleigh-Taylor problem at different times; (a) present study; (b) Popinet and Zaleski (1999)

3.1.2 Rayleigh-Taylor problem with velocity perturbation. As another kind of perturbation, two viscous incompressible fluid layers with a density ratio of two and a uniform kinematic viscosity in a rectangular domain is investigated as shown in Figure 8. A single wavelength perturbation is introduced by using the following velocity field which is adopted from the work of Kelecy and Pletcher (1997):

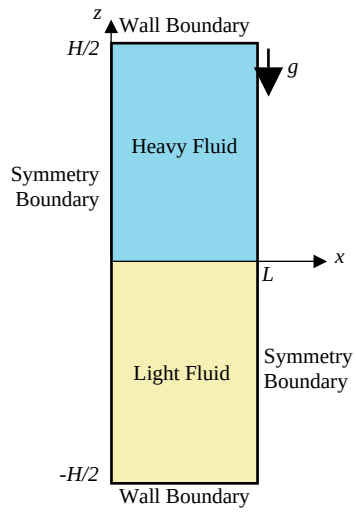

Figure 8.
Illustration of Rayleigh-Taylor problem with velocity perturbation

$$\frac{u}{V_r} = \begin{cases} \alpha \sin\left(\frac{\pi x}{L}\right) \exp\left(-\frac{\pi |y|}{L}\right) & \frac{y}{L} > 0 \\ -\alpha \sin\left(\frac{\pi x}{L}\right) \exp\left(-\frac{\pi |y|}{L}\right) & \frac{y}{L} < 0 \end{cases} \tag{30}$$

$$\frac{v}{V_r} = \alpha \cos\left(\frac{\pi x}{L}\right) \exp\left(-\frac{\pi |y|}{L}\right) \quad \alpha = \frac{\pi A \Delta y}{2 V_r L}$$

where $V_r = \sqrt{gL}$, A is perturbation amplitude and Δy is a representative mesh increment in the vertical direction. This perturbation corresponds to a sinusoidal perturbation of wavelength *2L*.

To verify the accuracy of current study, the problem is simulated for $Re = (\rho_r V_r L)/\mu_r = 28.3$ where all variables replace from the heavy fluid. Results show a good concordance by Kelecy and Pletcher (1997) (Figure 9). Here, a non-dimensional time $T = t\sqrt{g/L}$ is used.

The effect of Re number on the evolution of free surface is shown in Figure 10 for the same time. In all cases, the initial perturbation causes the light fluid to rise along the left boundary and the heavy fluid to sink along the right boundary. During the early times, it is considered that the displacement of the interface is nearly symmetric. Anyway, the roll up of the interface is much more pronounced for higher *Re* number due to the smaller influence of viscosity, which would tend to smooth out sharp velocity gradients.

3.2 Sloshing

Sloshing of a liquid wave with a low amplitude under the influence of gravity has been investigated (Tadjbakhsh and Keller, 1960) and used as a test to evaluate the interface (Raad *et al.*, 1995). The situation with an initialized quiescent fluid free surface is shown in Figure 11, which is the same as used by Raad *et al.* The domain is discretised

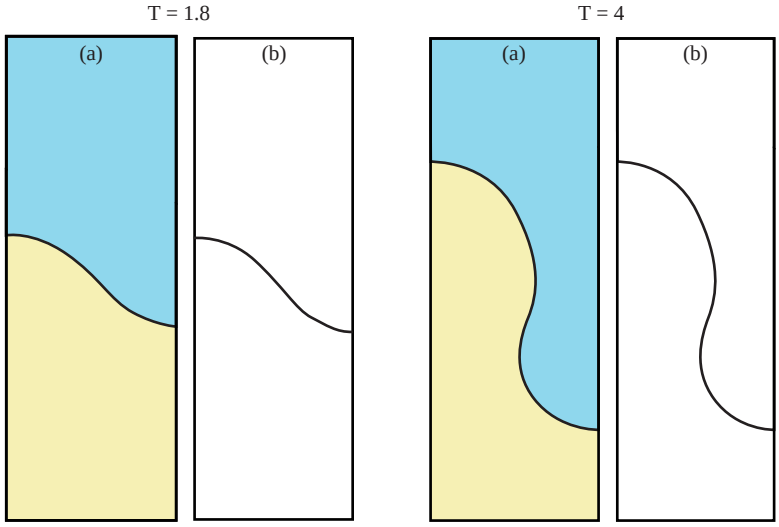

Figure 9.
Rayleigh-Taylor at different times; (a) present study; (b) Kelecy and Pletcher (1997)

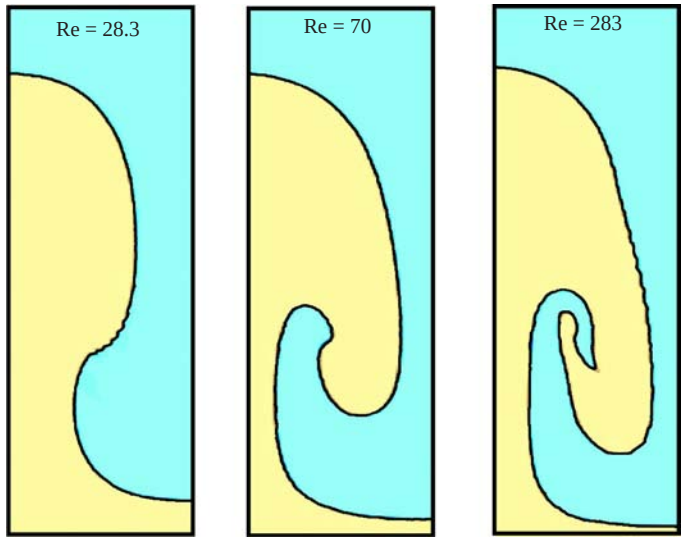

Figure 10.
Effect of Re number in Rayleigh-Taylor at the same time of $T = 4.8$

with 160 cells in the horizontal direction and 104 cells in the vertical direction. Slip and zero-gradient boundary conditions are used for velocity and pressure at all boundaries, respectively. In this case, fluid begins to slosh solely under the influence of constant gravitational field. The theoretical period of sloshing of the first mode is $T = 2\pi\sqrt{gk\tanh(kh)} = 0.3739\,\mathrm{s}$, where k is the wave number and h the average fluid depth (Raad *et al.*, 1995).

Initially the whole system is at rest. After a quarter of a period the potential energy of the system is transferred to kinetic energy and the velocities reach their maximum.

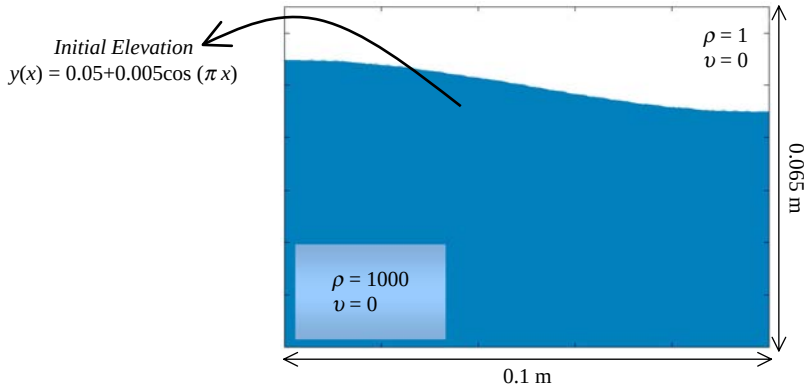

Figure 11.
Initial geometry of the sloshing problem

After a half period, all the kinetic energy is transferred back into potential energy with the velocity almost back to zero (Figure 12). Also, Figure 13 shows plots of the position of the interface at the left boundary against time. The frequency corresponds with the theoretical one, so do the amplitudes of even periods.

3.3 Dam breaking

A classical experiment used in the validation of mathematical modeling of two-fluid system, is the collapse of liquid column. Figure 14 shows the sketch of primary experimental setup (Martin and Moyce, 1952). There are some secondary data such as reduction of the column height (z) and progression of column front (x) to validate numerical calculations. The specific geometry employed in the present work is

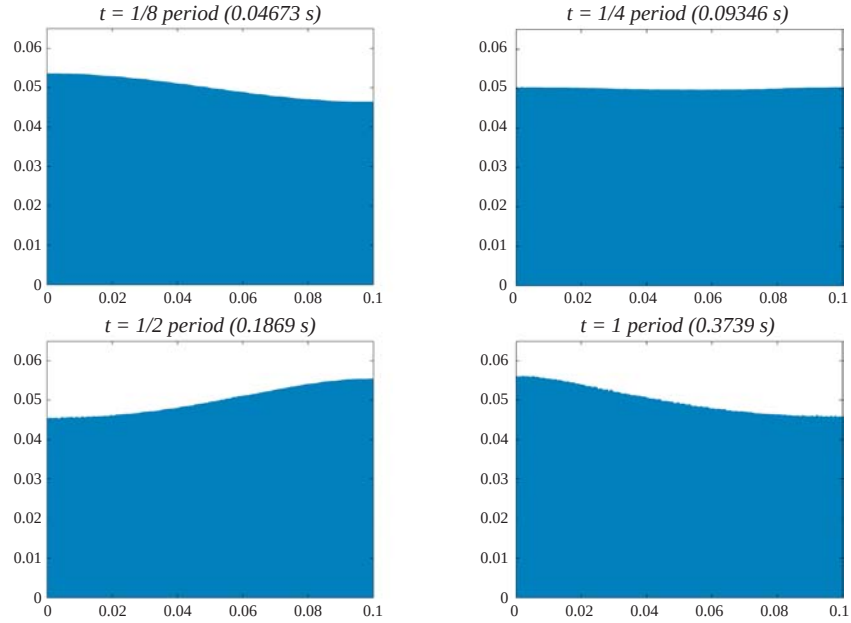

Figure 12.
Plots of the wave position for the first period of the sloshing

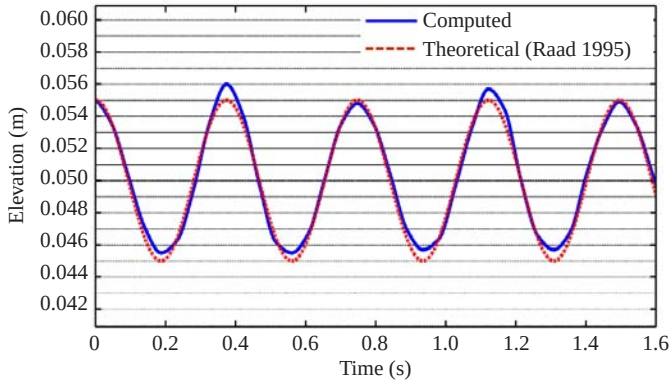

Figure 13.
Position of the interface at the left boundary

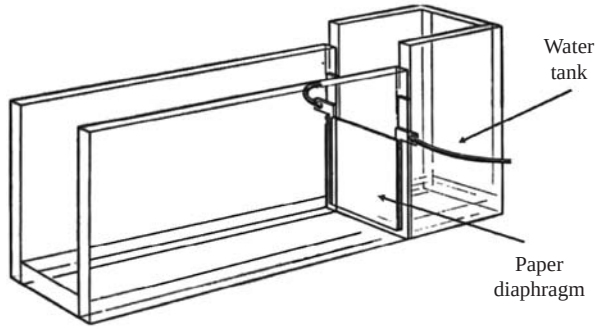

Figure 14.
Diagram of a typical apparatus in dam breaking experimental setup (Martin and Moyce, 1952)

shown in Figure 15 where $a = 0.05715$ m. The calculation is made by using a uniform grid of 40×160 and $20 \times 20 \times 80$ cell for two- and three-dimensional cases, respectively.

No-slip boundary condition for velocity and zero-gradient condition for pressure are used on whole walls. The snapshots of free surface motion are plotted in Figures 16 and 17 for such cases. The surge front and the column height (in three-dimensional

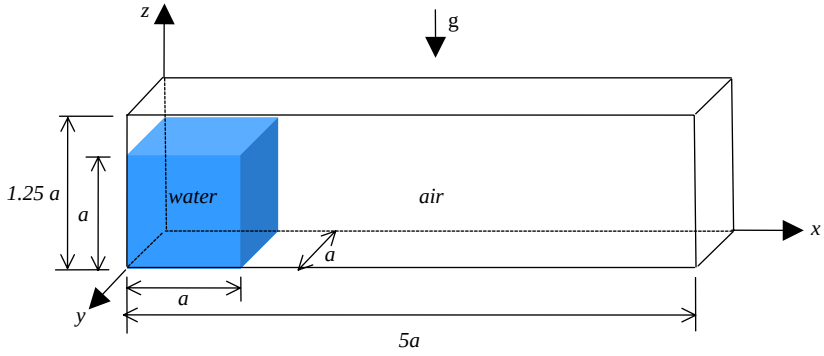

Figure 15.
Illustration of dam breaking

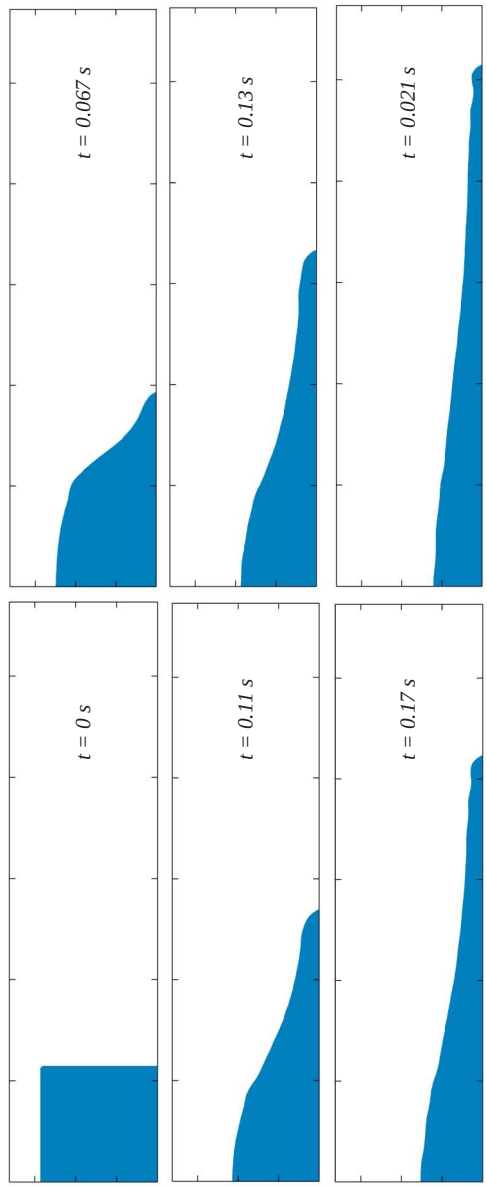

Figure 16.
Free surface motion in two-dimensional case

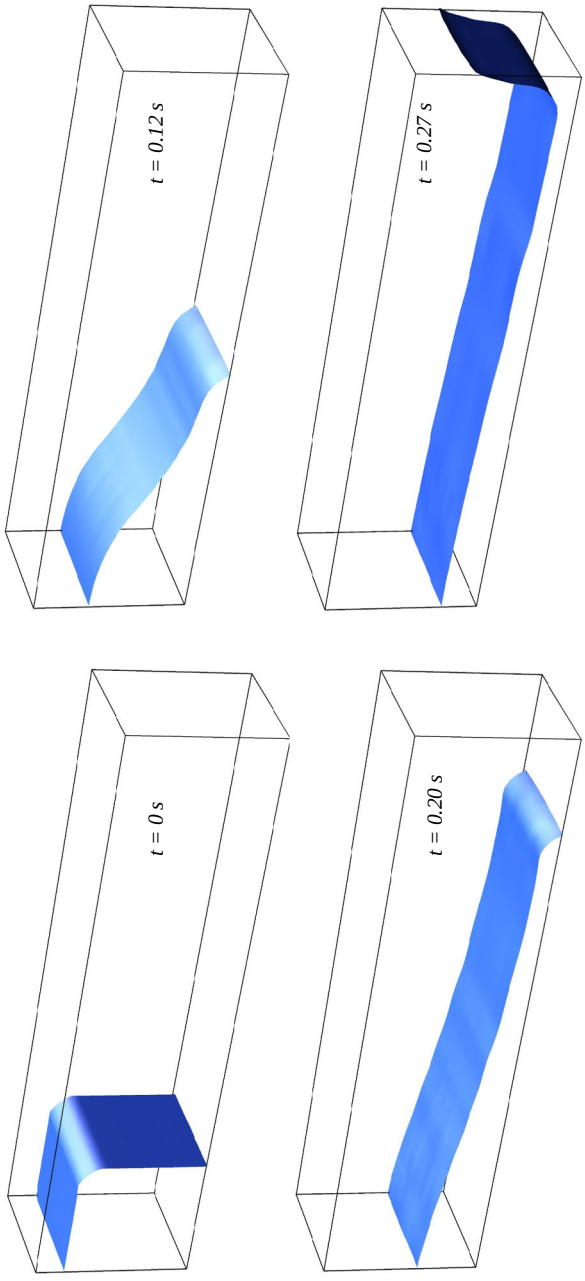

Figure 17.
Free surface motion in three-dimensional case

case at the symmetry plane) are plotted in Figures 18 and 19. Also plotted in these figures are the experimental data of Martin and Moyce (1952).

Figures appear that the numerical results are in good agreement with experiment. However, the simulation seems to be ahead of the physical data with respect to the position of the leading edge. One implies that the unsynchronized start of simulation and physical data leads to such a shift (Croce *et al.*, 2004). In addition, the important point is that the current simulation ignores the effect of surface tension which exists in physics. Besides, there is very little difference between two- and three-dimensional simulations, which is clear in such plots. It is probably due to the high Reynolds number for this particular case, which reduces the influence of side walls on the flow

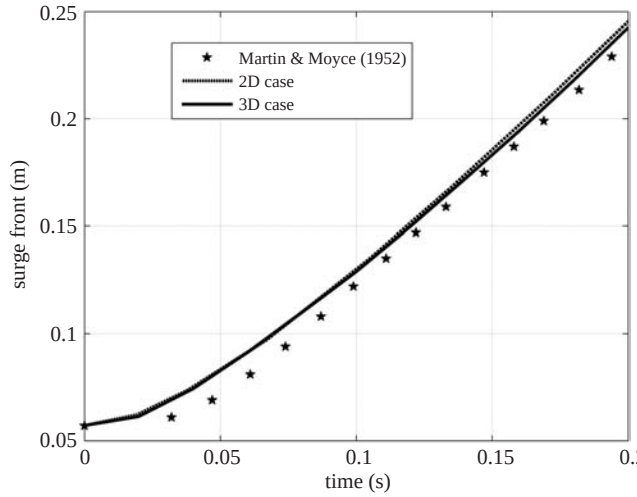

Figure 18.
Surge front position

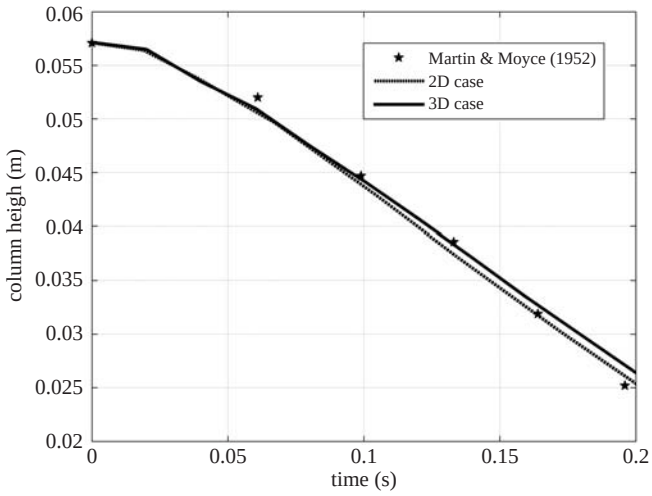

Figure 19.
Column height

field at the symmetry plane. It seems that the surge front and the column height are changing linearly a bit after the beginning of the collapse.

A more interesting version of dam breaking occurs when a small obstacle is placed in the way of the water front as shown in Figure 20 (Koshizuka *et al.*, 1995). In this case, considering the flow of both water and air is important because air is trapped in water. Here, the trapped-air is subjected to a large buoyancy force and tends to rise up. This is obvious from Figure 21 which shows the shape of a water column at three time instants. Comparison of numerical data and experimental photos of Figure 21 shows a good concordance.

4. Conclusion

The preceding sections have described the development of a three-dimensional finite volume two phase flow solver. The algorithm employs the fractional step method to couple both velocity and pressure fields in a transient flow. An appropriate interface capturing scheme is selected for simulation of the complex deformations. To discretise the free surface scalar transport equation which calculates the volume fraction distribution, a high resolution differencing scheme is applied to avoid non-physical values. The use of a consistent formulation in both the liquid and gas regions permits the free surface to be automatically captured as a discontinuity in the density and viscosity, and thereby eliminates the need for special free surface tracking procedure, although this discontinuity must be treated in a special manner. A new pressure interpolation method is presented for this purpose which strongly eliminates velocity oscillation at interface, especially when there are two fluids with high density ratio, e.g. air and water.

An extensive set of validation calculations were carried out for two-and three-dimensional test cases and comparison of the results shows a reasonably good agreement between numerical and experimental data.

Although the presented method has been tested by using simple geometries, the formulation is of sufficient generality to permit free surface flows in more complex geometries to be computed.

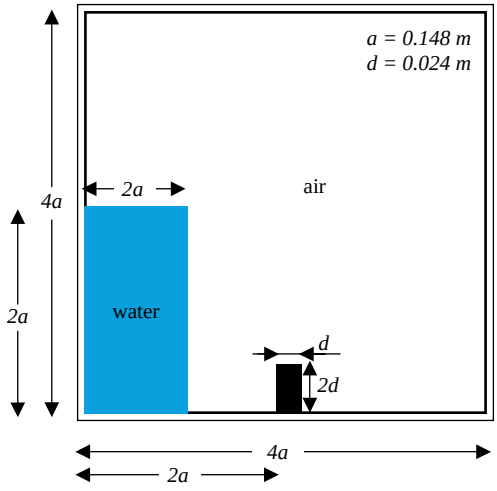

Figure 20.
Illustration of dam breaking with an obstacle

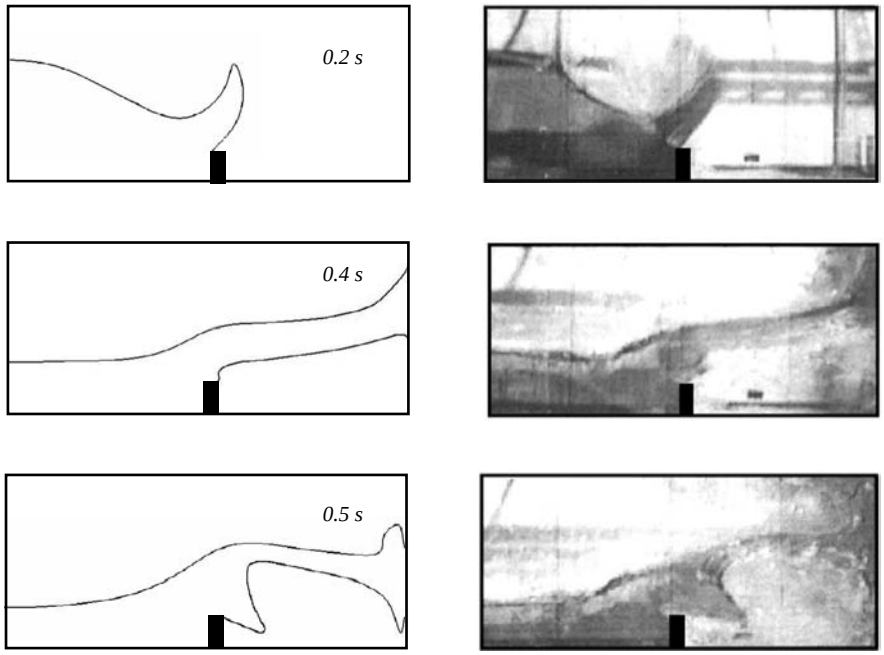

Figure 21.
Comparison of the numerical simulation of the present study (left) by experimental visualization of Koshizuka *et al.* (1995) (right)

References

Bell, J.B., Collela, P. and Howell, H. (1991), "An efficient second-order projection method for viscous incompressible flow", *Proceeding of tenth AIAA Computational Fluid Dynamics Conference, AIAA*, p. 360.

Biausser, B., Fraunie, P., Grilli, S. and Marcer, R. (2004), "Numerical analysis of the internal kinematics and dynamics of three-dimensional breaking waves on slopes", *Int. J. of Offshore and Polar Eng.*, Vol. 14 No. 4.

Brown, D.L., Cortez, R. and Minion, M.L. (2001), "Accurate projection methods for the incompressible Navier-Stokes equations", *J. of Comput. Phys.*, Vol. 168, pp. 464-99.

Chen, G. and Kharif, C. (1999), "Two-dimensional Navier-Stokes simulation of breaking waves", *Phys. of Fluids*, Vol. 11 No. 1, pp. 121-33.

Chorin, A.J. (1968), "Numerical solution of the Navier-Stokes equations", *Math. Comput.*, Vol. 22, p. 745.

Chorin, A.J. (1969), "On the convergence of discrete approximations to the Navier-Stokes equations", *Math. Comput.*, Vol. 23, p. 341.

Croce, R., Griebel, M., Schweitzer, M.A. (2004), "A parallel level-set approach for two-phase flow problems with surface tension in three space dimensions", (*Journal of Computational Physics*) Preprint 157, Sonderforschungsbereich 611, Universitat Bonn.

Dendy, E.D., Padial-Collins, N.T. and VanderHeyden, W.B. (2002), "A general-purpose finite-volume advection scheme for continuous and discontinuous fields on unstructured grids", *J. of Comput. Phys.*, Vol. 180, pp. 559-83.

Fekken, G., Veldman, A.E.P. and Buchner, B. (1999), "Simulation of green water loading using the Navier-Stokes equations", *Proceeding of the 7th Int. Conference on Numerical Ship Hydrodynamics, Nantes, France*.

Ferziger, J.H. and Peric, M. (2002), *Computational Methods for Fluid Dynamics*, 3rd ed., Springer, New York, NY.

Gaskell, H. and Lau, A.K.C. (1988), "Curvature-compensated convective transport: SMART, a new boundedness-preserving transport algorithm", *Int. J. of Num. Methods in Fluids*, Vol. 8, pp. 617-41.

Goda, K. (1979), "A multiphase technique with implicit difference schemes for calculating two- or three- dimensional cavity flows", *J. Comput. Phys.*, Vol. 30, p. 76.

Huijsmans, R.H.M. and Van Grosen, E. (2004), "Coupling freak wave effects with green water simulations", *Proceeding of the 14th ISOPE, Toulon, France, 23-28 May*.

Issa, R.I. (1986), "Solution of the implicitly discretised fluid flow equations by operator-splitting", *J. of Comput. Phys.*, Vol. 62 No. 1, pp. 40-65.

Jahanbakhsh, E., Panahi, P. and Seif, M.S. (2005), "Multi-dimensional free surface flow simulation using two-phase Navier-Stokes solver", *Proceeding of 8th Numerical Towing Tank Symposium (NuTTs), Varna, 2-4 October*.

Jasak, H. (1996), "Error analysis and estimation for finite volume method with application to fluid flows", PhD thesis, University of London, London.

Kelcey, F.J. and Pletcher, R.H. (1997), "The development of free surface capturing approach for multidimensional free surface flows in closed containers", *J. of Comput. Phys.*, Vol. 138, pp. 939-80.

Kim, D. and Choi, H. (2000), "A second-order time-accurate finite volume method for unsteady incompressible flow on hybrid unstructured grids", *J. of Comput. Phys.*, Vol. 162, pp. 411-28.

Kim, J. and Moin, P. (1985), "Application of a fractional-step method to incompressible Navier-Stokes equations", *J. Comput. Phys.*, Vol. 59, p. 308.

Koshizuka, S., Tamako, H. and Oka, Y. (1995), "A particle method for incompressible viscous flow with fluid fragmentation", *Comput. Fluid Dynamics J.*, Vol. 4 No. 1, pp. 29-46.

Leonard, B.P. (1979), "Stable and accurate convective modeling procedure based on quadratic upstream interpolation", *Comp. Meth. in Appl. Mech. and Eng.*, Vol. 19, pp. 59-98.

Leonard, B.P. (1991), "The ULTIMATE conservation difference scheme applied to unsteady one dimensional direction", *Comp. Meth. in Appl. Mech. and Eng.*, Vol. 88, pp. 17-74.

Loots, E., Buchner, B., Pastoor, W. and Tveitnes, T. (2004), "The numerical solution of LNG sloshing with an improved volume-of-fluid method", *Proceeding of 23rd Int. Conference on Offshore Mech. And Arctic Eng. (OMAE2004-51085), Vancouver*.

Martin, J.C. and Moyce, W.J. (1952), "An experimental study of the collapse of liquid columns on a rigid horizontal plane", *Philos. Trans. Roy. Soc. London*, Vol. A244, pp. 312-24.

Muzaferija, S. and Peric, M. (1998), "Computation of free surface flows using interface tracking and interface capturing methods", in Mahrenholtz, O. and Markiewicz, M. (Eds), *Nonlinear Water Waves Interaction*, Chapter 2, Computational Mechanics Publications, Southhampton.

Panahi, R., Jahanbakhsh, E. and Seif, M.S. (2005), "Comparison of interface capturing methods in two phase flow", *Iranian Journal of Science & Technology, Transaction B: Technology*, Vol. 29, No. B6.

Patankar, S.V. and Spalding, D.B. (1972), "A calculation procedure for heat, mass and momentum transfer in three dimensional parabolic flows", *Int. J. of Heat and Mass Transfer*, Vol. 15, p. 1787.

Popinet, S. and Zaleski, S. (1999), "A front tracking algorithm for accurate representation of surface tension", *Int. J. of Num. Meth. in Fluids*, Vol. 30, pp. 775-93.

Puckett, E.G., Almgren, A.S., Bell, J.B., Marcus, D.L. and Rider, W.J. (1997), "A high order projection method for tracking fluids interfaces in variable density incompressible flows", *J. of Comput. Phys.*, Vol. 100, pp. 269-82.

Raad, P.E., Chen, S. and Johnson, D.B. (1995), "The introduction of micro cells to treat pressure in free surface fluid flow problems", *J. of Fluids Eng.*, Vol. 117, pp. 683-90.

Scardovelli, R. and Zaleski, S. (1999), "Direct numerical simulation of free-surface and interfacial flow", *Annual Review of Fluid Mechanics*, Vol. 31, pp. 567-603.

Spalding, D.B. (1974), "A method for computing steady and unsteady flows possessing discontinuities of density", CHAM Report 910/2.

Tadjbakhsh, I. and Keller, J.B. (1960), "Standing surface waves of finite amplitude", *J. of Fluid Mech.*, Vol. 8, pp. 442-51.

Ubbink, O. (1997), "Numerical prediction of two fluid systems with sharp interfaces", PhD thesis, Department of Mechanical engineering, Imperial College, London.

Ubbink, O. and Issa, R.I. (1999), "A method for capturing sharp fluid interfaces on arbitrary meshes", *J. of Comput. Phys.*, Vol. 153, pp. 26-50.

Van Kan, J. (1986), "A second-order accurate pressure-correction scheme for viscous incompressible flow", *SIAM, J. Sci. Comput.*, Vol. 7, p. 870.

Versteeg, H.K. and Malalasekera, W. (1995), *An Introduction to Computational Fluid Dynamics, the Finite Volume Method*, Longman scientific & Technical, Harlow.

Yang, C., Lohner, R. and Yim, S.C. (2005), "Development of a CFD simulation method for extreme wave and structure interactions", *Proceeding of 24th Int. Conference on Offshore Mech. and Arctic Eng. (OMAE2005), Halkidiki, Greece, 12-17 June*.

Zang, Y., Street, R.L. and Kossef, J.R. (1994), "A non-staggered grid, fractional step method for time-dependent incompressible Navier-Stokes equations in curvilinear coordinates", *J. of Comput. Phys.*, Vol. 114, pp. 18-33.

Corresponding author
M.S. Seif can be contacted at: seif@sharif.edu

To purchase reprints of this article please e-mail: **reprints@emeraldinsight.com**
Or visit our web site for further details: **www.emeraldinsight.com/reprints**